THE JOURNAL OF PHYSICAL CHEMISTRY C

Article

pubs.acs.org/JPCC

# Effect of Pore Confinement of $LiNH_2$ on Ammonia Decomposition Catalysis and the Storage of Hydrogen and Ammonia

Peter L. Bramwell, Sarah Lentink, Peter Ngene, and Petra E. de Jongh*

Inorganic Chemistry and Catalysis, Debye Institute for Nanomaterials Science, Utrecht University, Universiteitsweg 99, Utrecht, The Netherlands 3583CG

Supporting Information

**ABSTRACT:** $LiNH_2$ is of interest to several aspects of energy storage such as reversible hydrogen storage, battery technology, catalysis, and ammonia capture/storage. We investigated the impact of nanoconfinement in carbon scaffolds on the hydrogen and ammonia release properties of $LiNH_2$ and its catalytic activity in $NH_3$ decomposition. Ammonia release from macrocrystalline $LiNH_2$ begins at 350 °C, while confined $LiNH_2$ releases ammonia from below 100 °C under helium flow. This ammonia release consisted of 30.5 wt % ammonia in the first cycle and was found to be partially reversible. Above 300 °C, hydrogen is also released due to an irreversible reaction between $LiNH_2$ and the carbon support to form $Li_2NCN$. Ni-doped $LiNH_2$/C nanocomposites were active in the catalytic decomposition of ammonia into $N_2$ and $H_2$ with 53% conversion at 400 °C and a gas hourly space velocity of 13000 $h^{-1}$. This is comparable to the performance of a commercial-type Ru-based catalyst where 79% conversion is observed under the same conditions. This work demonstrates that nanoconfinement is effective for improving the functionality of $LiNH_2$. The versatility of this system offers promise in a number of different areas including hydrogen/ammonia storage and ammonia decomposition catalysis.

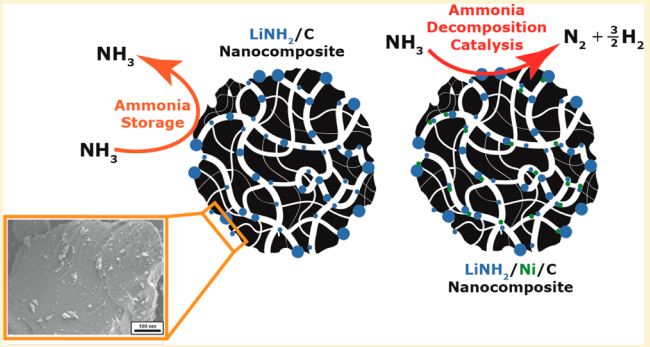


## 1. INTRODUCTION

$LiNH_2$ has garnered a great deal of interest in a number of energy storage applications. Reversible hydrogen storage is a prime example as $LiNH_2$ can store 6.5 wt % hydrogen, which is released through its decomposition to $Li_2NH$ (Scheme 1).[1−9]

**Scheme 1. Possible Equilibria of Lithium Amide**[2]

| | | |
|---|---|---|
| (1) | $2LiNH_2 \leftrightarrow Li_2NH + NH_3$ | ($\Delta H$ = 84 kJ $mol^{-1}$ $NH_3$) |
| (2) | $LiH + NH_3 \rightarrow LiNH_2 + H_2$ | ($\Delta H$ = -39 kJ $mol^{-1}$ $H_2$) |
| (3) | $Li_2NH + LiH \leftrightarrow Li_3N + H_2$ | ($\Delta H$ = 165 kJ $mol^{-1}$ $H_2$) |

However, there are several drawbacks of this system for hydrogen storage, the first being the high temperature required to release hydrogen at a reasonable rate, approximately 300 °C.

The second drawback is the generation of ammonia during decomposition,[10−14] which is a poison for fuel cells.[8] Ammonia release can be prevented by mixing LiH with $LiNH_2$ so that the LiH rapidly captures the released ammonia to form $LiNH_2$ and $H_2$ gas. The reaction between $LiNH_2$ and LiH has been extensively studied in order to minimize the ammonia release and maximize the hydrogen release. Studies have shown that a 1:1 mixture of $LiNH_2$ and LiH is optimum and the two components must be thoroughly mixed to prevent ammonia release.[15]

On the other hand, this ammonia release could be exploited in the storage of ammonia gas for indirect storage of hydrogen.[16−18] The decomposition of ammonia to yield hydrogen and nitrogen has recently garnered a lot of interest due to the fact that high-purity hydrogen can be produced in situ from ammonia, which already has an extensive transport and storage infrastructure in place.[17] A study on the use of $LiNH_2$ in ammonia decomposition indicated that the active phase was in fact $Li_2NH$, which is formed upon decomposition of $LiNH_2$.[18] As the decomposition of $LiNH_2$ only occurs at temperatures above 300 °C, catalytic activity is only observed at 350 °C and above. Although this is comparable to the commercially utilized Ru/alumina catalyst and the recently studied $NaNH_2$,[19] the temperatures required for full conversion of ammonia are still very high. Progress in this field has also been made through the use of doping $Li_2NH$ with transition metal nitrides, where a ternary nitride is formed.[20−22] A range of ternary nitrides were tested from Ti to Cu, where Mn demonstrated the highest activity at temperatures above 327 °C.[21]

Reduction of the particle size, or nanosizing, is an established strategy for improving the kinetics, for instance, for hydrogen

**Received:** October 25, 2016
**Revised:** November 11, 2016
**Published:** November 14, 2016






DOI: 10.1021/acs.jpcc.6b10688
J. Phys. Chem. C 2016, 120, 27212−27220

Table 1. Summary of Data Determined from Nitrogen Physisorption for the Nanocomposites Prepared on the CX27 and NPG Supports[a]

| | BET surface area/ $m^2\ g^{-1}$ | micropore volume/ $cm^3\ ^3\ g^{-1}g^{-1}$ | micropore volume loss[b]/$cm^3\ g^{-1}$ | mesopore volume/ $cm^3\ g^{-1}$ | mesopore volume loss/ $cm^3\ g^{-1}$ | estimated particle size/nm |
|---|---|---|---|---|---|---|
| CX27 | 604 | 0.17 | | 0.64 | | |
| $LiNH_2$/CX27 | 77 | 0.01 | 0.16 | 0.20 | 0.44 | 4−40 |
| Ni/CX27 | 484 | 0.17 | 0.00 | 0.60 | 0.04 | 2−12[c] |
| $LiNH_2$/Ni/CX27 | 122 | 0.01 | 0.16 | 0.34 | 0.30 | 4−40 |
| NPG | 17 | 0.00 | | 0.05 | | |
| $LiNH_2$/NPG | 19 | 0.00 | 0.00 | 0.05 | 0.00 | |

[a]Particle size distributions were calculated by subtracting the pore size distribution of the nanocomposite from that of the support after leaching of the $LiNH_2$. [b]Micropores are easily blocked; therefore, this micropore volume loss is likely at least partially due to pore-blocking. [c]Determined from TEM.

release from light metal hydrides.[23,24] Interaction between the metal hydride and carbon-based supports gives an additional reduction in hydrogen release temperatures.[25−28] Nanosizing has been applied to several systems such as $LiBH_4$,[29] $MgH_2$,[30,31] and $NaAlH_4$[32,33] supported on carbon. However, there are very few examples of the preparation of supported nanoparticles of $LiNH_2$. This may be because the preparation of such materials is far from trivial. Techniques such as melt infiltration are not applicable for $LiNH_2$ as it decomposes before melting; however, there are a few examples of alternative preparation strategies being found.[34−36] Nanocomposites can be prepared by solution impregnation, but the low solubility of $LiNH_2$ and other components of the system severely limits the use of this method in this case. An alternative is to use precursors that can be subsequently transformed to $LiNH_2$. Impregnation of $LiN_3$, which can be decomposed to form $Li_3N$, is an example from the literature.[36] The resulting $Li_3N$/C nanocomposite can reversibly absorb 9 wt % hydrogen to form $LiNH_2$ and decomposes back to $Li_3N$ at 300 °C.

We have previously reported a method for preparing carbon-supported LiH particles through impregnation with butyllithium with a range of sizes and demonstrated that nanoconfinement has a large influence on the hydrogen release profile.[37] In this article, we present a procedure for the preparation of $LiNH_2$/C nanocomposites. We build on the solution impregnation using butyllithium to produce LiH particles,[38] which can then be treated with gaseous ammonia to yield $LiNH_2$ particles. We show that nanoconfinement in nanoporous carbon has a remarkable effect on the properties of $LiNH_2$ in energy storage applications including reversible ammonia storage, hydrogen storage, and for the catalytic decomposition of ammonia into nitrogen and hydrogen.

## 2. EXPERIMENTAL SECTION

**2.1. Materials.** All materials were stored in an argon-filled glovebox (Mbraun Labmaster dp, 1 ppm $H_2O$, <1 ppm of $O_2$) with the exception of the butyllithium solution, which was stored in a nitrogen-filled glovebox (Mbraun Labmaster I30, 1 ppm $H_2O$, <1 ppm of $O_2$). $LiNH_2$ (95%, hydrogen storage grade), *tert*-butyllithium (1.7 M in pentane) solution, and citric acid (anhydrous) were purchased from Sigma-Aldrich. Nickel(II) nitrate hexahydrate (99%) was purchased from Acros Organics. All gases were obtained from Linde with a purity of 99.9999% for hydrogen and 99.998% for ammonia. Two different carbon supports were used: carbon xerogel and nonporous graphite (NPG). The carbon xerogel support was prepared using the sol−gel resorcinol procedure[39] with a mixture of formaldehyde, resorcinol, sodium carbonate, and deionized water. After aging, the resulting red solid was ground, crushed, and washed with acetone before pyrolizing at 800 °C for 10 h under argon flow to obtain the black xerogel. CX27 (average pore size of 27 nm with a distribution from 4 to 40 nm) was obtained in this manner. The pores were characterized using nitrogen physisorption. NPG was obtained from TimCal and dried under argon flow at 600 °C for 12 h before use. NPG is nonporous and has a surface area of 20 $m^2\ g^{-1}$.

**2.2. Nanocomposite Preparation.** The $LiNH_2$/C nanocomposites were prepared by mixing 10 mL of the *t*-butyllithium solution and 1 g of carbon support in an autoclave (Parr, 50 mL) while inside of a nitrogen-filled glovebox. The autoclave was then heated, with stirring, for 20 h under 50 bar of hydrogen pressure at 100 °C. After cooling to room temperature, the remaining gas was vented and vacuum applied via a cold trap for 2 h to remove solvent. The autoclave was then pressurized with 8 bar of ammonia and left to settle for 1 h before venting the ammonia and repressurizing with ammonia two more times to ensure complete conversion of LiH to $LiNH_2$, resulting in a $LiNH_2$ loading of 27 wt %. In order to confirm that the pore structure was not affected by the impregnation procedure, the $LiNH_2$ was removed from each nanocomposite by soaking in 1 M HCl solution overnight, drying in an oven at 120 °C overnight, and remeasuring the porosity by nitrogen physisorption.

In the preparation of the $LiNH_2$/Ni/C nanocomposite, nickel(II) nitrate hexahydrate and citric acid were mixed in a 3:2 molar ratio and dissolved in demineralized water. The carbon support was then impregnated with the volume of solution equivalent to the pore volume of the support and dried under vacuum for 2 h at 120 °C before reduction under 5% $H_2$ in $N_2$ flow at 350 °C (heating rate of 2 °C $min^{-1}$) for 30 min. The resulting supported nickel nanoparticles were characterized by X-ray diffraction (XRD) and transmission electron microscopy (TEM, performed using a Tecnai 12 instrument operating at 120 kV). The average Ni particle size was 6−7 nm (from TEM). This Ni/C material was then impregnated with $LiNH_2$ in the same manner as described above. For details of the characterization, see Supporting Information Figure S1.3.

**2.3. X-ray Diffraction.** XRD measurements were performed by a Bruker AXS D8 advance 120 machine (Co−$K_\alpha$ radiation, airtight sample holder used). The crystallite sizes of $LiNH_2$ in each nanocomposite were determined from the peak width of the $LiNH_2$ XRD peak at $2\theta$ = 35° according to the Scherrer method.[40] The degree of crystallinity of $LiNH_2$ in each nanocomposite was determined by reference to the measured $LiNH_2$/C physical mixtures. The ratio of the peak intensity for the peak at $2\theta$ = 35° ($LiNH_2$) to the intensity of the peak at $2\theta$


DOI: 10.1021/acs.jpcc.6b10688
J. Phys. Chem. C 2016, 120, 27212−27220

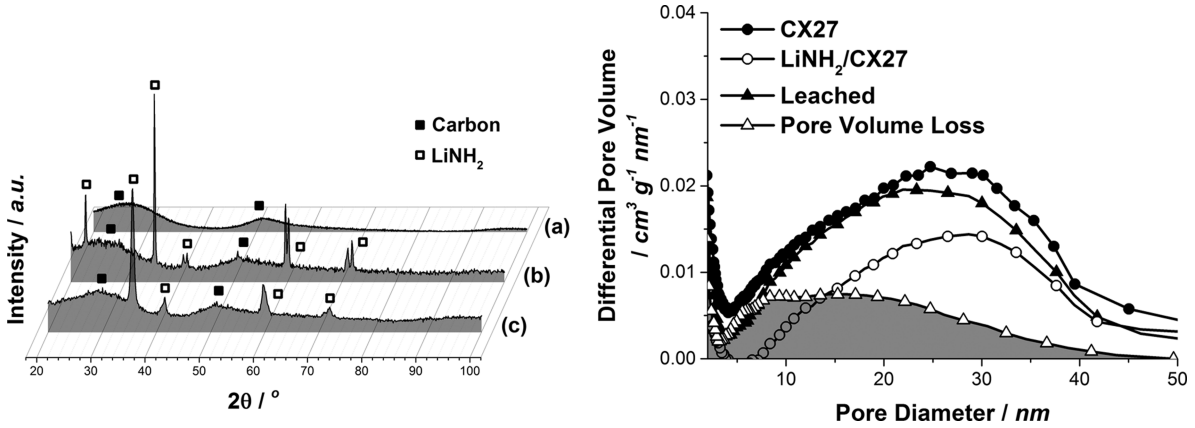


**Figure 1.** Left: XRD patterns for (a) the carbon xerogel support (CX27) before impregnation, (b) a $LiNH_2$/CX27 physical mixture, and (c) the $LiNH_2$/CX27 nanocomposite in the as-prepared state. Each pattern is normalized to the main carbon peak (at around 30°) in each sample. Right: Pore size distributions obtained from nitrogen physisorption for CX27, the $LiNH_2$/CX27 nanocomposite, and the nanocomposite following leaching.

= 30° (carbon support) was calculated for the physical mixture and for the nanocomposite. The degree of crystallinity was then calculated by taking the ratio from the nanocomposite as a percentage of the ratio from the physical mixture.

**2.4. Nitrogen Physisorption.** Nitrogen physisorption was performed at 77 K using a Micromeritics TriStar instrument. Micropore volumes (<2 nm) were calculated using the t-plot method. The mesopore volumes (the 2−300 nm range) and Barrett−Joyner−Halenda (BJH) pore size distributions of the support and nanocomposites were determined using the adsorption branch of the isotherm with carbon black as a reference.

Information about the particle size of the $LiNH_2$ in the nanocomposites was obtained by subtracting the pore size distribution of the nanocomposite from that of the corresponding leached sample. In this way, the volume of the pores of a certain size lost upon $LiNH_2$ deposition was determined, which is a rough indication of the particle size of the $LiNH_2$ particles contained within these pores. All of these data are summarized for the supports and nanocomposites in Table 1.

**2.5. Scanning Electron Microscopy.** SEM was performed using an FEI XL30 FEG SEM instrument in backscattered electron mode. Samples were passivated in air and coated with an 8 nm layer of Pt before measurement. $LiNH_2$ particles were observed by comparison to the pristine support material; however, observation of the particles was only possible in the CX27-supported nanocomposites as the difference in morphology between the CX27 support and $LiNH_2$ allowed suitable visual contrast between the $LiNH_2$ and the carbon. This was not the case for the $LiNH_2$/NPG nanocomposite (Supporting Information section S1). The particle sizes mentioned in this paper were determined by measuring the sizes of at least 500 particles per sample and calculating the average.

**2.6. Temperature-Programmed Desorption.** TPD measurements were performed with a Micromeritics AutoChem II, equipped with a TCD detector; this was coupled to a calibrated Hiden QIC series gas analysis system during measurement to distinguish between hydrogen ($m/z$ = 2), ammonia ($m/z$ = 17), and nitrogen ($m/z$ = 28). For each measurement, roughly 50 mg of sample was used under an Ar flow of 25 mL $min^{-1}$, heating to 600 °C at a rate of 5 °C $min^{-1}$.

**2.7. Ammonia Storage Measurements.** Ammonia storage measurements were also carried out in the Micromeritics AutoChem II apparatus. Measurements were carried out using 100 mg of material and consisted of two alternating steps: desorption and absorption. The desorption step was carried out by heating to 250 °C at a rate of 5 °C $min^{-1}$ under 25 mL $min^{-1}$ He flow and maintaining 250 °C for 10 min. The absorption step was carried out by flowing 10% $NH_3$ in He over the sample at a flow rate of 50 mL $min^{-1}$ while the sample was maintained at room temperature for 1 h. Successive cycles were performed by alternating between these two steps and cooling to ambient temperature under 25 mL $min^{-1}$ flow of He in between each step. The desorption and absorption cycles as well as reference measurements to determine the influence of nanoconfinement on the reversibility of ammonia sorption can be found in Supporting Information section S2.

**2.8. Hydrogen Uptake Measurements.** Hydrogen uptake was measured using a Sievert type apparatus (PCT Pro-2000, Hy-Energy & Setaram; pressure measurement accuracy: 1% of reading) using 100 mg of sample. Desorption prior to measurement was performed at 350 °C with a temperature ramp of 5 °C $min^{-1}$, a hold time of 30 min, and Ar flow of 25 mL $min^{-1}$. Hydrogen absorption was performed by pressurizing the sample with 50 bar of hydrogen in 0.1 bar intervals at 200 °C and measuring the rate of hydrogen uptake by monitoring the pressure decrease over time. The total molar quantity of hydrogen absorbed was calculated as a gravimetric quantity from the recorded pressure drop at each pressure increment.

**2.9. Ammonia Decomposition.** The catalysis of the decomposition of ammonia was measured by loading the TPD-MS instrument with roughly 100−250 mg of catalyst. The sample was heated to 600 °C at a temperature ramp of 5 °C $min^{-1}$ under a 25 mL $min^{-1}$ flow of 10% $NH_3$ in He. The amount of sample used varied for each material depending on its density, but in each case, enough was used to give a gas hourly space velocity (GHSV) of roughly 13000 $h^{-1}$. The gas was analyzed using the mass analyzer to follow the concentrations of $NH_3$, $H_2$, and $N_2$ in the gas stream. The degree of ammonia conversion was measured by monitoring the reduction in the intensity of the $NH_3$ signal, which was compared to the increase in intensity of the $H_2$ and $N_2$ signals to confirm that ammonia decomposition was occurring. For example, if the hydrogen signal increased in intensity but no nitrogen was observed in the gas flow, then it could be


DOI: 10.1021/acs.jpcc.6b10688
J. Phys. Chem. C 2016, 120, 27212−27220

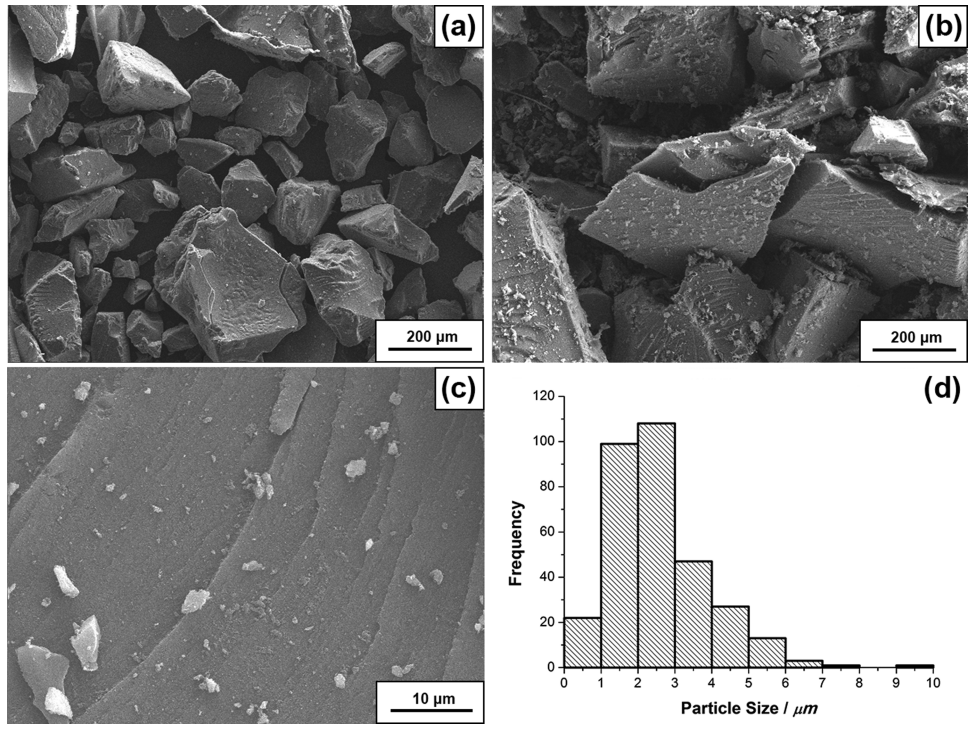


**Figure 2.** SEM images for (a) the CX27 support, (b,c) $LiNH_2$/CX27, and (d) a histogram representing the $LiNH_2$ particle size distribution. Samples were passivated in air and coated with 8 nm of Pt before imaging.

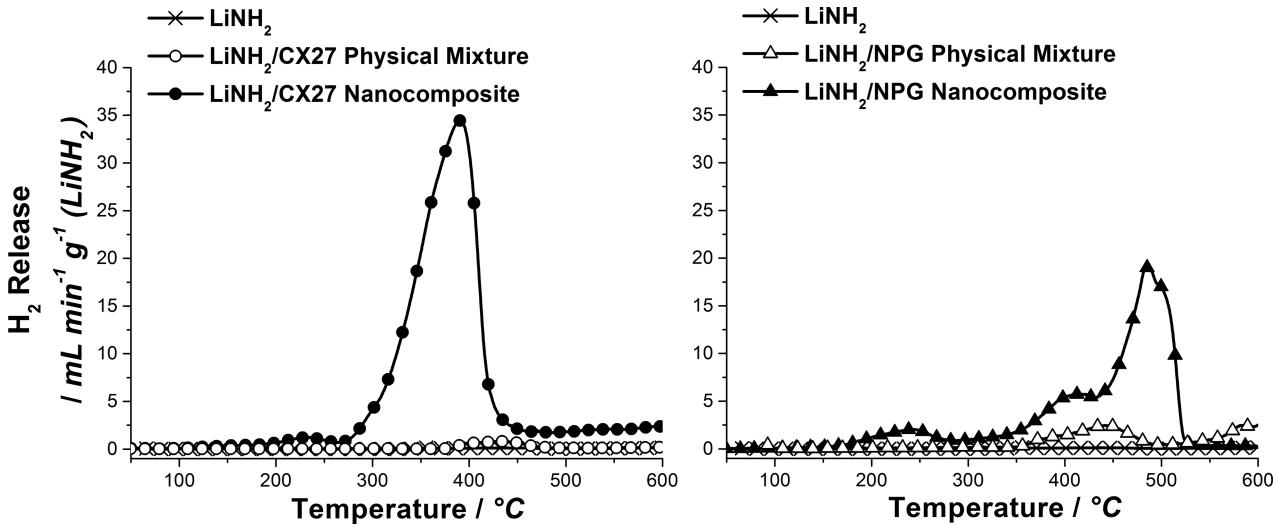


**Figure 3.** Hydrogen release profiles measured for the $LiNH_2$/CX27 (left) and $LiNH_2$/NPG (right) nanocomposites compared to the bulk $LiNH_2$ powder and their physical mixtures with the carbon supports. One in 25 data points is shown.

concluded that ammonia decomposition was not occurring but rather a side reaction that produces hydrogen. For comparison to the $LiNH_2$/C and $LiNH_2$/Ni/C nanocomposites, a commercially available catalyst composed of Ru particles supported on alumina (5 wt % Ru loading, 1−2 nm particles, 128 $m^2\ g^{-1}$ BET surface area) was measured as well as carbon-supported Ni particles at a loading of 5 wt % of Ni. For a blank measurement, an empty reactor was also measured under the same conditions. As a means of determining the stability of the $LiNH_2$/Ni/C catalyst, a sample was measured by heating 100 mg of sample under a 50 mL $min^{-1}$ flow of 10% $NH_3$ in He to 200 °C at 5 °C $min^{-1}$ with a 1 h hold time. The temperature was then increased to 300 °C for 1 h, then to 400 °C for 1 h, and was once again reduced to 300 °C for 1 h, and this cycle was repeated one more time (for more details, see Supporting Information section S4).

## 3. RESULTS AND DISCUSSION

**3.1. Structural Characterization.** Figure 1 shows the XRD pattern of the $LiNH_2$/CX27 nanocomposite as well as those of the xerogel support and the $LiNH_2$/CX27 physical mixture as a reference. The $LiNH_2$ crystallite size in the physical mixture is larger than 30 nm and therefore cannot be accurately determined. For the nanocomposite, the peak at 36° is clearly broader, with an estimated crystallite size of 27 nm. This suggests that smaller particles are present compared to the


DOI: 10.1021/acs.jpcc.6b10688
J. Phys. Chem. C 2016, 120, 27212−27220

physical mixture. Note that the smallest particles lack long-range crystallinity and hence are not visible in the XRD pattern. It can therefore be assumed that the amount of $LiNH_2$ detected by XRD corresponds to the amount of $LiNH_2$ not confined to the carbon pores. The $LiNH_2$/CX27 nanocomposite has a degree of crystallinity of 56%, which suggests that 44% of the $LiNH_2$ is confined to the carbon pores. However, as the pores of the carbon support are relatively large, some of the particles confined to the pores may exhibit crystallinity, and therefore, this figure should be considered as the lower limit of the quantity of confined $LiNH_2$.

Nitrogen physisorption (Figure 1, right) shows a pore volume loss in the range of 4−40 nm, suggesting that the $LiNH_2$ in the pores of the $LiNH_2$/CX27 nanocomposite has a feature size distribution ranging from 4 to 40 nm. The pore volume loss is higher than the total volume of $LiNH_2$ added, which suggests a significant degree of pore blocking in both the micro- and mesopores.

Direct observation of the particles on the external surface of the support is possible using scanning electron microscopy (SEM), shown in Figure 2. The $LiNH_2$ particles are visible with sizes ranging from 1 to 6 $\mu$m with an average at 3 $\mu$m. It can be concluded that there are two types of $LiNH_2$ particles in the $LiNH_2$/CX27 nanocomposite, those in the range of 4−40 nm that are contained within the carbon pores and those a few micrometers in size located on the outer surface of the support.

**3.2. Hydrogen Release.** $LiNH_2$ releases ammonia and hydrogen upon decomposition.[2] Hence, we studied the decomposition behavior of the nanocomposites and physical mixtures using TPD-MS (Figure 3). A large hydrogen release peak is observed when heating the $LiNH_2$/CX27 nanocomposite between 300 and 400 °C, amounting to 4.9 wt % with respect to $LiNH_2$. This hydrogen release peak is not observed in the bulk powder at all, but it is observed in the physical mixture, although only 0.2 wt % of hydrogen is released (hydrogen and ammonia release quantities are summarized in Table 2). This suggests that the presence of the carbon may be the reason for the hydrogen release. XRD following treatment at 300 °C (Supporting Information Figure S3.1) shows the formation of $Li_2NCN$ and the loss of most of the $LiNH_2$. Therefore, it can be concluded that the hydrogen release between 300 and 400 °C is in fact due to a reaction between the carbon support and $LiNH_2$. The fact that a larger amount of hydrogen is released in the nanocomposites compared to the physical mixtures supports this as the smaller particles in the nanocomposites have a greater degree of contact with the carbon and therefore would yield more reaction between $LiNH_2$ and carbon. This observation shows that close contact between the carbon and $LiNH_2$ facilitates hydrogen release from $LiNH_2$. Unfortunately, there was no substantial hydrogen uptake by the dehydrogenated samples even at 50 bar of $H_2$ and 200 °C, which shows that the formation of $Li_2NCN$ is not easily reversed (Supporting Information section S3).

**Table 2. Overview of the Temperatures and Quantities of Hydrogen Release from the Nanocomposites and Their Corresponding Physical Mixtures**

| material | temperature of $H_2$ release/°C[a] | $H_2$ release/wt % ($LiNH_2$) |
|---|---|---|
| $LiNH_2$ | (342) 444 | 0.1 |
| $LiNH_2$/CX27 physical mixture | (353) 418 | 0.2 |
| $LiNH_2$/CX27 nanocomposite | (274) 388 | 4.9 |
| $LiNH_2$/NPG physical mixture | (255) 400 | 0.4 |
| $LiNH_2$/NPG nanocomposite | (139) 237, 406, 507 | 3.5 |

[a]The number in parentheses is the lowest temperature of onset of release; the other numbers are temperatures at the peak of release.

In order to determine the influence of nanoconfinement, the $LiNH_2$/CX27 nanocomposite was compared to another nanocomposite prepared on NPG. As the NPG support has very little pore volume, all of the $LiNH_2$ in the nanocomposite can be considered to be on the external surface of the support. Therefore, any gas release observed can be attributed to nonconfined $LiNH_2$. This $LiNH_2$/NPG nanocomposite shows two hydrogen release peaks (Figure 3), which can be attributed to reaction with the carbon support. The reason for the presence of two peaks is not clear, but it may be due to small amounts of $LiNH_2$ confined to what little pore volume (0.05 $cm^3\ g^{-1}$) the framework has.

**3.3. Ammonia Release.** The ammonia release (Figure 4 and Table 3) shows a large difference between the physical mixtures and the nanocomposites. The $LiNH_2$/CX27 nanocomposite shows two ammonia release peaks: one peak at an onset temperature similar to that of the $LiNH_2$/NPG nanocomposite (starting at roughly 200 °C) but one other peak at a much lower temperature of roughly 100 °C. This low-temperature ammonia release is likely due to decomposition of $LiNH_2$ into $Li_2NH$ and $NH_3$, as seen in reaction (1) of Scheme 1.[5] The low-temperature ammonia release of 15.6 wt % may originate from the pore-confined $LiNH_2$, and the higher-temperature peak (14.9 wt %) originates from the nonconfined $LiNH_2$. According to the degree of crystallinity from the XRD data, at least 44% of $LiNH_2$ is confined within the CX27 nanocomposite, and 51% of the total ammonia release from the sample is released from pore-confined $LiNH_2$, which is in accordance with the lower limit established from XRD. The fact that confinement is essential for low-temperature ammonia release is evidenced by comparison to the $LiNH_2$/NPG nanocomposite where only high-temperature ammonia release is observed and a similar amount of ammonia (33.6 wt %) to the $LiNH_2$/CX27 nanocomposite is released. The temperature of this release is very similar to the physical mixture and the high temperature peak in the $LiNH_2$/CX27 nanocomposite. The $LiNH_2$/NPG nanocomposite has ammonia release roughly 50 °C lower than the physical mixture, which is likely due to the formation of smaller crystallites in the nanocomposite compared to those in the physical mixture.

The low temperature of ammonia release is very striking, and it is important to determine to what extent this release is reversible. Figure 5 shows the ammonia release over eight successive cycles with desorption performed up to 250 °C. Although reversible ammonia uptake can be clearly seen, the capacity reduces during each cycle, with a release of 30.5 wt % (with respect to $LiNH_2$) in the first cycle and eventually dropping to 1.0 wt % in the eighth cycle. XRD of the sample after cycling shows the presence of $Li_2O$ (Supporting Information Figure S2.3), demonstrating significant oxidation during or following the ammonia sorption cycles, which explains the capacity loss. The oxidation observed is likely to be due to the presence of small amounts of impurities in the gas stream and/or oxidation during handling and hence might be avoided by purifying the gas stream further. The average



DOI: 10.1021/acs.jpcc.6b10688
J. Phys. Chem. C 2016, 120, 27212−27220

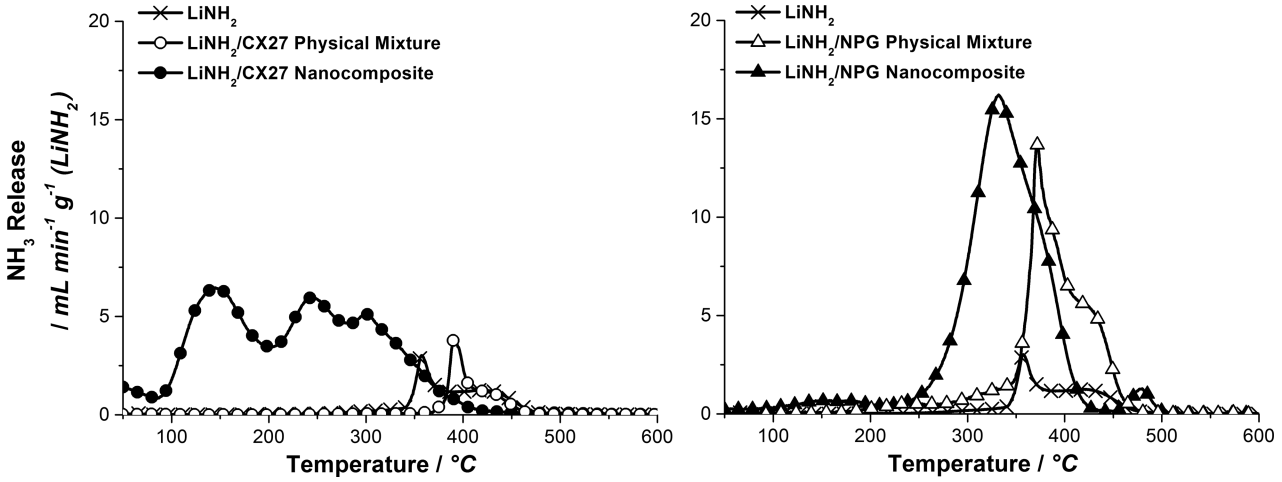


**Figure 4.** Ammonia release profiles measured for the $LiNH_2$/CX27 (left) and $LiNH_2$/NPG (right) nanocomposites compared to the bulk $LiNH_2$ powder and their physical mixtures with the carbon supports. One in 25 data points is shown.

**Table 3. Overview of the Temperatures and Quantities of Ammonia Release from the Nanocomposite and the Corresponding Physical Mixtures**

| material | temperature of $NH_3$ release/°C[a] | $NH_3$ release/wt % ($LiNH_2$) |
|---|---|---|
| $LiNH_2$ | (241), 356 | 1.0 |
| $LiNH_2$/CX27 physical mixture | (203) 373 | 2.7 |
| $LiNH_2$/CX27 nanocomposite | (40) 125, 322 | 30.5 |
| $LiNH_2$/NPG physical mixture | (142) 306, 352 | 17.1 |
| $LiNH_2$/NPG nanocomposite | (105) 156, 341 | 33.6 |

[a]The number in parentheses is the lowest temperature of onset of release; the other numbers are temperatures at the peak of release.

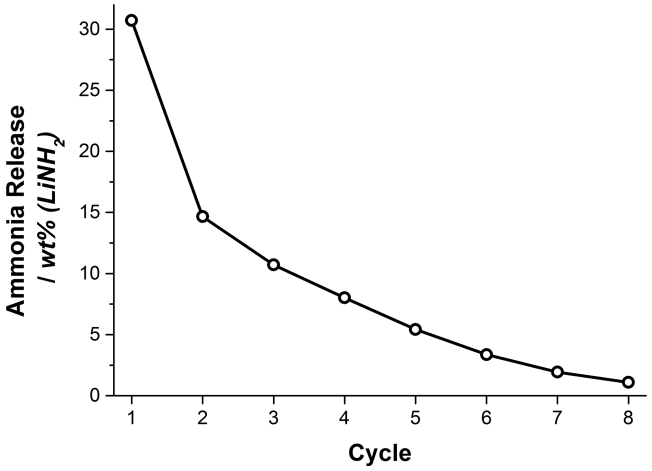


**Figure 5.** Quantity of ammonia desorbed over eight cycles for the $LiNH_2$/CX27 nanocomposite. Desorption performed under 50 mL $min^{-1}$ of He flow at a heating rate of 5 °C $min^{-1}$ to 250 °C with a 10 min hold time. Absorption was performed by flowing 10% $NH_3$ in He over the sample for 1 h at room temperature at a rate of 50 mL $min^{-1}$.

crystallite size of $LiNH_2$ increases from 17 to 24 nm during cycling. However, this change in crystallite size is highly unlikely to be the reason for the capacity drop but rather is symptomatic of the oxidation of the smaller $LiNH_2$ particles. Smaller particles are more susceptible to oxidation, and therefore, it is logical that only the larger particles remain after performing the cycles. As these larger particles release ammonia at higher temperatures, this would explain the capacity drop because the nanocomposite is only heated to 250 °C during cycling.

**3.4. Ammonia Decomposition Catalysis.** It has been reported that the decomposition of ammonia into hydrogen and nitrogen can be catalyzed by $Li_2NH$, which is formed through the decomposition of $LiNH_2$.[18] This is interesting as $Li_2NH$ could possibly replace the expensive Ru catalyst that is currently used for this process. However, macrocrystalline $LiNH_2$ decomposes above 300 °C, which means that high temperatures are required in order to observe high activity. As the $LiNH_2$ nanocomposite decomposes at temperatures 200 °C lower than the macrocrystalline system, it is plausible that it will exhibit catalytic activity at lower temperatures. In addition, the small size of the particles of $LiNH_2$ could boost activity further by providing a higher active surface area. For this reason, the $LiNH_2$ nanocomposite was tested as a catalyst for the ammonia decomposition reaction, the results of which are shown in Figure 6. For each experiment, a GHSV of 13000 $h^{-1}$ was used.

The $LiNH_2$/C nanocomposite and $LiNH_2$/C physical mixture do not show activity in the decomposition of ammonia. The macrocrystalline $LiNH_2$ shows 3% conversion at 300 °C, 13% at 400 °C, and 100% at 600 °C. Because there is no activity in the presence of carbon, it is likely that the aforementioned reaction between $LiNH_2$ and carbon is the reason for the lack of activity in the nanocomposite and physical mixture. This is supported by the significant amount of hydrogen that is observed above 350 °C (Figure 7). As no nitrogen is observed, which should form upon ammonia decomposition, it can be concluded that the hydrogen release is in fact due to reaction between $LiNH_2$ and carbon to form $Li_2NCN$.

Transition metals are known to boost the activity of Li-based materials in the ammonia decomposition reaction;[21] therefore, a nanocomposite composed of $LiNH_2$ doped with 5 wt % of Ni (average Ni particle size of 6−7 nm) was prepared (Figure S1.3), which is referred to as the $LiNH_2$/Ni/CX27 nanocomposite. Interestingly, the Ni-doped nanocomposite demonstrates clear activity starting from 300 °C with 53% conversion at 400 °C. As nickel itself is also known to be active in ammonia


DOI: 10.1021/acs.jpcc.6b10688
J. Phys. Chem. C 2016, 120, 27212−27220

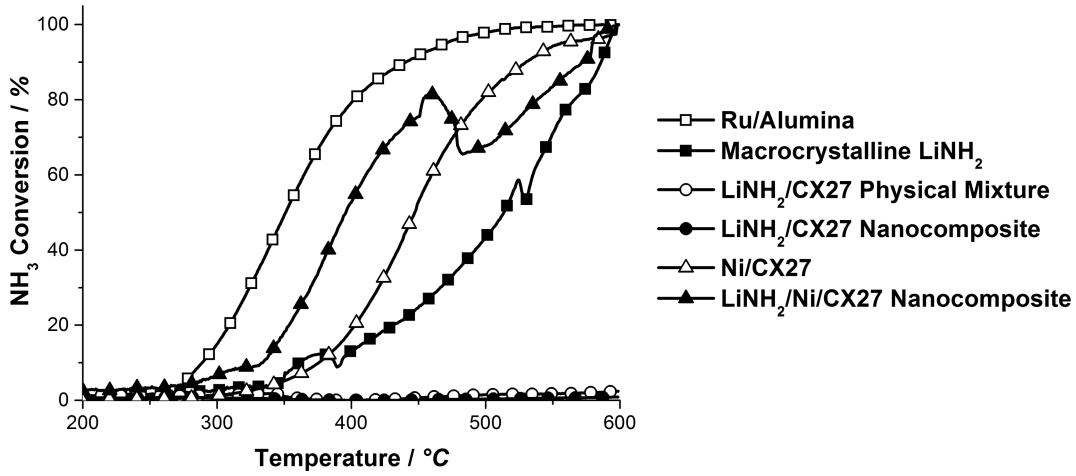


**Figure 6.** Ammonia conversion profile of the various catalysts tested in the decomposition of ammonia, determined from the concentration of nitrogen in the gas stream and performed by heating roughly 100−250 mg of catalyst in a TPD-MS instrument to 600 °C at 5 °C $min^{-1}$ under 50 mL $min^{-1}$ of 10% $NH_3$ in He flow (GHSV of 13000 $h^{-1}$).

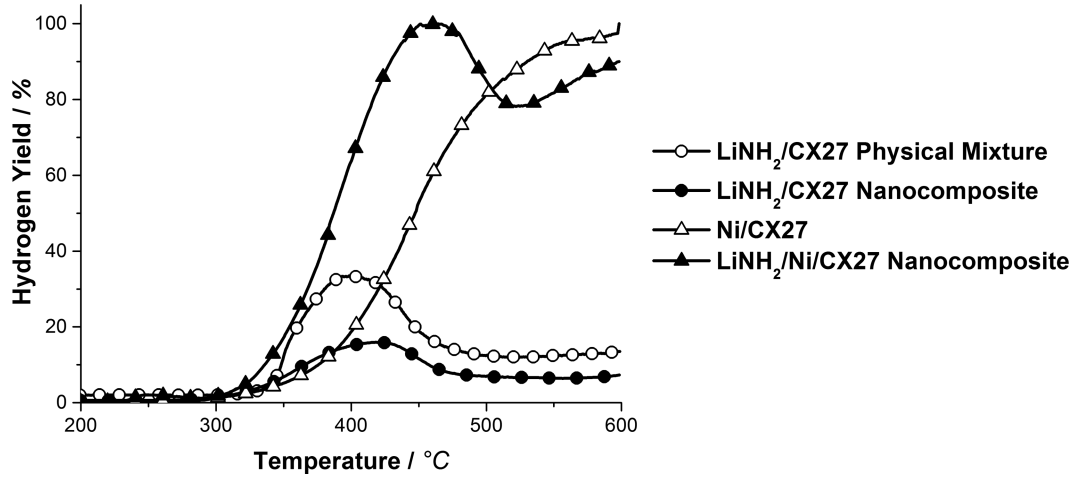


**Figure 7.** Hydrogen yield of the various catalysts tested in the decomposition of ammonia. This study was performed by heating 100−250 mg of catalyst in a TPD-MS instrument to 600 °C at 5 °C $min^{-1}$ under 50 mL $min^{-1}$ of 10% $NH_3$ in He flow (GHSV of 13000 $h^{-1}$).

decomposition catalysis,[18] a 5 wt % Ni/C (average Ni particle size of 6−7 nm) sample was also tested in order to determine the role of nickel in the activity of the catalyst. Ni/C shows 19% conversion at 400 °C, 34% lower than that of the $LiNH_2$/Ni/C nanocomposite. Therefore, it can be concluded that the combination of Ni and $LiNH_2$ is essential for such a high activity. The reason for this improved activity is expected to be similar to that found in ternary transition metal nitrides formed with $Li_2NH$ where the Li component helps to stabilize the metal−N bond to drive the ammonia decomposition reaction.[21]

There is a noticeable drop in ammonia conversion for the $LiNH_2$/Ni/C catalyst at around 450 °C. This likely originates from the reaction of $LiNH_2$ with the carbon support (Supporting Information section S4). Despite this, the $LiNH_2$/Ni/C catalyst compares favorably to other established catalysts. A commercial catalyst, namely, Ru/alumina (5 wt % Ru loading, 1−2 nm particles), displays ammonia conversion of 15% at 300 °C (at a GHSV of 13000 $h^{-1}$), while $LiNH_2$/Ni/C displays a conversion of 7% at the same temperature. At 400 °C, the ammonia conversion is 79 and 53% for the Ru/alumina and $LiNH_2$/Ni/C catalysts, respectively. Although the Ru/alumina catalyst has a higher activity than the $LiNH_2$/Ni/C nanocomposite, the particle sizes are very different. The Ru particles are 1−2 nm in size, while the $LiNH_2$ particles are in the range of 4−40 nm, with a significant portion on the micron scale. Therefore, it should be expected that the $LiNH_2$/Ni/C nanocomposite would be capable of achieving similar, or even higher, conversion should the $LiNH_2$ particle size be further reduced. This discovery of a new class of catalyst that has comparable activity to that of a commercial catalyst should help to advance the growing field of ammonia decomposition catalysis.

## 4. CONCLUSION

A nanocomposite of carbon-supported $LiNH_2$ nanoparticles has been prepared by treating pore-confined LiH particles with ammonia gas at room temperature. Both ammonia and hydrogen are emitted during decomposition under heating. The hydrogen release, which begins at 300 °C, was irreversible due to reaction between the support and $LiNH_2$. The ammonia release occurred at much lower temperatures (starting from 50 °C) compared to the physical mixture and bulk system (both 300 °C). This ammonia release of up to 30.5 wt % was partially reversible but reduced upon cycling probably due to oxidation of the material.



DOI: 10.1021/acs.jpcc.6b10688
J. Phys. Chem. C 2016, 120, 27212−27220

Finally, doping of the confined $LiNH_2$ with Ni produced a material that was able to catalyze the decomposition of ammonia at temperatures of 300−400 °C at conversion rates comparable to that of a commonly used Ru-based catalyst (5 wt %, 1−2 nm particles, supported on alumina) and faster than that for carbon-supported 6 nm Ni particles. A conversion of 7% is observed at 300 °C and 53% at 400 °C (GHSV of 13000 $h^{-1}$), with deactivation at higher temperatures, possibly due to reaction with the support. In comparison, the Ru/alumina catalyst displays conversion of 15% at 300 °C and 79% at 400 °C. Further work is required to reduce the $LiNH_2$ particle size, but this material shows great promise in the storage of ammonia and hydrogen as well as ammonia decomposition, demonstrating the striking versatility of the confined $LiNH_2$ system for energy storage applications.

## ■ ASSOCIATED CONTENT

### Supporting Information

The Supporting Information is available free of charge on the ACS Publications website at DOI: 10.1021/acs.jpcc.6b10688.

Procedures, characterization data, calculations, and other data mentioned in the text (PDF)

## ■ AUTHOR INFORMATION


### Corresponding Author

*E-mail: P.E.dejongh@uu.nl.

### ORCID

Petra E. de Jongh: 0000-0002-2216-2620


### Author Contributions

The manuscript was written through contributions of all authors. All authors have given approval to the final version of the manuscript.

### Notes

The authors declare no competing financial interest.

## ■ ACKNOWLEDGMENTS

The authors would like to acknowledge Prof. Dr. Ir. Krijn de Jong for scientific discussions on the topic, Rien van Zwienen and Jan-Willem de Rijk for technical support, as well as Jochem Wijten, Nynke Krans, Lisette Pompe, and Marjan Versluis for SEM and TEM measurements. The authors would also like to thank The Netherlands Organization for Scientific Research (NWO-ECHO, Grant Number 712.012.004) for funding the project.

## ■ ABBREVIATIONS

TPD, temperature-programmed desorption; SEM, scanning electron microscopy; TEM, transmission electron microscopy; MS, mass spectrometry; XRD, X-ray diffraction; CX27, carbon xerogel with average pore diameter of 27 nm; NPG, nonporous graphite; GHSV, gas hourly space velocity

## ■ REFERENCES


(1) Sakintuna, B.; Lamari-Darkrim, F.; Hirscher, M. Metal Hydride Materials for Solid Hydrogen Storage: A Review. *Int. J. Hydrogen Energy* **2007**, *32*, 1121−1140.

(2) Chen, P.; Xiong, Z.; Luo, J.; Lin, J.; Tan, K. L. Interaction of Hydrogen with Metal Nitrides and Imides. *Nature* **2002**, *420*, 302−304.

(3) Zaginaichenko, S. Y.; Matysina, Z. A.; Schur, D. V.; Zolotarenko, A. D. Li-N-H System − Reversible Accumulator and Store of Hydrogen. *Int. J. Hydrogen Energy* **2012**, *37*, 7565−7578.

(4) Xia, G.; Li, D.; Chen, X.; Tan, Y.; Tang, Z.; Guo, Z.; Liu, H.; Liu, Z.; Yu, X. Carbon-Coated $Li_3N$ Nanofibers for Advanced Hydrogen Storage. *Adv. Mater.* **2013**, *25*, 6238−6244.

(5) Leng, H. Y.; Ichikawa, T.; Hino, S.; Fujii, H. Investigation of Reaction between $LiNH_2$ and $H_2$. *J. Alloys Compd.* **2008**, *463*, 462−465.

(6) Lan, Z.; Jiang, W.; Bai, J.; Guo, J. The First-Principles Investigation on the Electronic Structure and Mechanism of LiH + $NH_3$ → $LiNH_2$ + $H_2$ Reaction. *Int. J. Hydrogen Energy* **2012**, *37*, 18937−18943.

(7) Lamb, J.; Chandra, D.; Chien, W.; Phanon, D.; Penin, N.; Černý, R.; Yvon, K. Mitigation of Hydrogen Capacity Losses during Pressure Cycling of the $Li_3N$−H System by the Addition of Nitrogen. *J. Phys. Chem. C* **2011**, *115*, 14386−14391.

(8) Gregory, D. H. Lithium Nitrides, Imides and Amides as Lightweight, Reversible Hydrogen Stores. *J. Mater. Chem.* **2008**, *18*, 2321.

(9) Jain, I. P.; Jain, P.; Jain, A. Novel Hydrogen Storage Materials: A Review of Lightweight Complex Hydrides. *J. Alloys Compd.* **2010**, *503*, 303−339.

(10) Hoang, K.; Janotti, A.; Van de Walle, C. G. Mechanisms for the Decomposition and Dehydrogenation of Li Amide/imide. *Phys. Rev. B: Condens. Matter Mater. Phys.* **2012**, *85*, 64115.

(11) Hu, Y. H.; Ruckenstein, E. Ultrafast Reaction between LiH and $NH_3$ during $H_2$ Storage in $Li_3N$. *J. Phys. Chem. A* **2003**, *107*, 9737−9739.

(12) Hino, S.; Ichikawa, T.; Ogita, N.; Udagawa, M.; Fujii, H. Quantitative Estimation of $NH_3$ Partial Pressure in $H_2$ Desorbed from the Li-N-H System by Raman Spectroscopy. *Chem. Commun.* **2005**, *24*, 3038−3040.

(13) Bonnet, M.-L.; Tognetti, V. The Influence of Density Functional Approximations on the Description of LiH + $NH_3$ → $LiNH_2$ + $H_2$ Reaction. *Chem. Phys. Lett.* **2011**, *511*, 427−433.

(14) Chen, P.; Xiong, Z.; Luo, J.; Lin, J.; Tan, K. L. Interaction between Lithium Amide and Lithium Hydride. *J. Phys. Chem. B* **2003**, *107*, 10967−10970.

(15) Yao, J. H.; Shang, C.; Aguey-Zinsou, K. F.; Guo, Z. X. Desorption Characteristics of Mechanically and Chemically Modified $LiNH_2$ and ($LiNH_2$ + LiH). *J. Alloys Compd.* **2007**, *432*, 277−282.

(16) Klerke, A.; Christensen, C. H.; Nørskov, J. K.; Vegge, T. Ammonia for Hydrogen Storage: Challenges and Opportunities. *J. Mater. Chem.* **2008**, *18*, 2304.

(17) Lan, R.; Irvine, J. T. S.; Tao, S. Ammonia and Related Chemicals as Potential Indirect Hydrogen Storage Materials. *Int. J. Hydrogen Energy* **2012**, *37*, 1482−1494.

(18) Makepeace, J. W.; Wood, T. J.; Hunter, H. M. A.; Jones, M. O.; David, W. I. F. Ammonia Decomposition Catalysis Using Non-Stoichiometric Lithium Imide. *Chem. Sci.* **2015**, *6*, 3805.

(19) David, W. I. F.; Makepeace, J. W.; Callear, S. K.; Hunter, H. M. a.; Taylor, J. D.; Wood, T. J.; Jones, M. O. Hydrogen Production from Ammonia Using Sodium Amide. *J. Am. Chem. Soc.* **2014**, *136*, 13082−13085.

(20) Guo, J.; Chen, Z.; Wu, A.; Chang, F.; Wang, P.; Hu, D.; Wu, G.; Xiong, Z.; Yu, P.; Chen, P. Electronic Promoter or Reacting Species? The Role of $LiNH_2$ on Ru in Catalyzing $NH_3$ Decomposition. *Chem. Commun.* **2015**, *51*, 15161−15164.

(21) Guo, J.; Wang, P.; Wu, G.; Wu, A.; Hu, D.; Xiong, Z.; Wang, J.; Yu, P.; Chang, F.; Chen, Z.; et al. Lithium Imide Synergy with 3d Transition-Metal Nitrides Leading to Unprecedented Catalytic Activities for Ammonia Decomposition. *Angew. Chem., Int. Ed.* **2015**, *54*, 2950−2954.

(22) Guo, J.; Chang, F.; Wang, P.; Hu, D.; Yu, P.; Wu, G.; Xiong, Z.; Chen, P. Highly Active MnN−$Li_2NH$ Composite Catalyst for Producing CO X -Free Hydrogen. *ACS Catal.* **2015**, *5*, 2708−2713.

(23) de Jongh, P. E.; Adelhelm, P. Nanosizing and Nanoconfinement: New Strategies towards Meeting Hydrogen Storage Goals. *ChemSusChem* **2010**, *3*, 1332−1348.

(24) Fichtner, M. Nanoconfinement Effects in Energy Storage Materials. *Phys. Chem. Chem. Phys.* **2011**, *13*, 21186−21195.




DOI: 10.1021/acs.jpcc.6b10688
J. Phys. Chem. C 2016, 120, 27212−27220

(25) Varin, R. A.; Jang, M. The Effects of Graphite on the Reversible Hydrogen Storage of Nanostructured Lithium Amide and Lithium Hydride ($LiNH_2$ + 1.2LiH) System. *J. Alloys Compd.* **2011**, *509*, 7143−7151.
(26) Wang, J.; Ebner, A. D.; Ritter, J. A. Kinetic Behavior of Ti-Doped $NaAlH_4$ When Cocatalyzed with Carbon Nanostructures. *J. Phys. Chem. B* **2006**, *110*, 17353−17358.
(27) Adelhelm, P.; de Jong, K. P.; de Jongh, P. E. How Intimate Contact with Nanoporous Carbon Benefits the Reversible Hydrogen Desorption from NaH and $NaAlH_4$. *Chem. Commun.* **2009**, *41*, 6261−6263.
(28) Adelhelm, P.; de Jongh, P. E. The Impact of Carbon Materials on the Hydrogen Storage Properties of Light Metal Hydrides. *J. Mater. Chem.* **2011**, *21*, 2417.
(29) Gross, A. F.; Vajo, J. J.; Van Atta, S. L.; Olson, G. L. Enhanced Hydrogen Storage Kinetics of $LiBH_4$ in Nanoporous Carbon Scaffolds. *J. Phys. Chem. C* **2008**, *112*, 5651−5657.
(30) de Jongh, P. E.; Wagemans, R. W. P.; Eggenhuisen, T. M.; Dauvillier, B. S.; Radstake, P. B.; Meeldijk, J. D.; Geus, J. W.; de Jong, K. P. The Preparation of Carbon-Supported Magnesium Nanoparticles Using Melt Infiltration. *Chem. Mater.* **2007**, *19*, 6052−6057.
(31) Nielsen, T. K.; Manickam, K.; Hirscher, M.; Besenbacher, F.; Jensen, T. R. Confinement of $MgH_2$ Nanoclusters Materials. *ACS Nano* **2009**, *3*, 3521−3528.
(32) Gao, J.; Ngene, P.; Lindemann, I.; Gutfleisch, O.; de Jong, K. P.; de Jongh, P. E. Enhanced Reversibility of $H_2$ Sorption in Nano-confined Complex Metal Hydrides by Alkali Metal Addition. *J. Mater. Chem.* **2012**, *22*, 13209.
(33) Gao, J.; Adelhelm, P.; Verkuijlen, M. H. W.; Rongeat, C.; Herrich, M.; van Bentum, P. J. M.; Gutfleisch, O.; Kentgens, A. P. M.; de Jong, K. P.; de Jongh, P. E. Confinement of $NaAlH_4$ in Nanoporous Carbon: Impact on $H_2$ Release, Reversibility, and Thermodynamics. *J. Phys. Chem. C* **2010**, *114*, 4675−4682.
(34) Hao, T.; Matsuo, M.; Nakamori, Y.; Orimo, S. Impregnation Method for the Synthesis of Li−N−H Systems. *J. Alloys Compd.* **2008**, *458*, L1−L5.
(35) Menjo, M.; Hyodo, Y.; Moriyama, S.; Li, H.-W.; Matsuo, M.; Semboshi, S.; Orimo, S. Cyclic Hydrogenation and Dehydrogenation Property of $LiNH_2$ Impregnated into Ni Foam. *Mater. Trans.* **2011**, *52*, 623−626.
(36) Demir-Cakan, R.; Tang, W. S.; Darwiche, A.; Janot, R. Modification of the Hydrogen Storage Properties of Li3N by Confinement into Mesoporous Carbons. *Energy Environ. Sci.* **2011**, *4*, 3625.
(37) Bramwell, P. L.; Ngene, P.; de Jongh, P. E. Carbon Supported Lithium Hydride Nanoparticles: Impact of Preparation Conditions on Particle Size and Hydrogen Sorption. *Int. J. Hydrogen Energy* **2016**, DOI: 10.1016/j.ijhydene.2016.10.062.
(38) Zhang, S.; Gross, A. F.; Van Atta, S. L.; Lopez, M.; Liu, P.; Ahn, C. C.; Vajo, J. J.; Jensen, C. M. The Synthesis and Hydrogen Storage Properties of a $MgH_2$ Incorporated Carbon Aerogel Scaffold. *Nanotechnology* **2009**, *20*, 204027.
(39) Al-Muhtaseb, S. A.; Ritter, J. A. Preparation and Properties of Resorcinol-Formaldehyde Organic and Carbon Gels. *Adv. Mater.* **2003**, *15*, 101−114.
(40) Langford, J. I.; Wilson, A. J. C. Scherrer after Sixty Years: A Survey and Some New Results in the Determination of Crystallite Size. *J. Appl. Crystallogr.* **1978**, *11*, 102−113.


DOI: 10.1021/acs.jpcc.6b10688
*J. Phys. Chem. C* 2016, 120, 27212−27220